Research Article

Improvement of the reactivity of soda–lime–silica glass solution as a hardener for producing geopolymer materials

Sorelle J. K. Melele[1] · Charles Banenzoué[2] · Daniel Fotio[3] · Hervé K. Tchakouté[1,4] · Claus H. Rüscher[4] · Charles P. N. Nanseu[5]

Abstract

The aiming target of this study is to improve the reactivity of the soda–lime–silica glass solution as a hardener for producing metakaolin-based geopolymer cements. The hardeners with molar ratios SiO_2/Na_2O equal to 1.5 from rice husk ash and waste glass were prepared. Due to the low dissolution of waste glass, the molar ratio SiO_2/Na_2O in soda–lime–silica glass solution is less than 1.5 suggesting thus the lower soluble silica content. In order to compensate for the deficiency of soluble silica in soda–lime–silica glass solution, the hardener from rice husk ash is added to the soda–lime–silica glass solution at different percentage such as 0, 20, 30, 40, 50, 60, 70, 80 and 100 wt%. The reactivity of the obtained hardeners was evaluated by using them for producing geopolymer cements. The X-ray pattern and infrared spectrum of residual waste glass indicate the higher intensity of the broad hump structure and the higher value of the wavenumber of the main band, respectively. This corresponds to the higher amount of glass phase contained in the residual waste glass. It was found that the values of the compressive strengths and the apparent density increase with increasing the addition of hardener from rice husk ash to the one from waste glass. The micrographs of geopolymer cements from hardeners containing 40, 50 and 100 wt% of sodium waterglass from rice husk ash are homogeneous and compact microstructure. This implies the formation of the higher connectivity and the long chain of poly(sialate-siloxo) network. The new approach for the preparation of a reactive hardener from the waste glass is found promising for the significant reduction of the greenhouse gas emitted during the production of geopolymers.

Graphic abstract

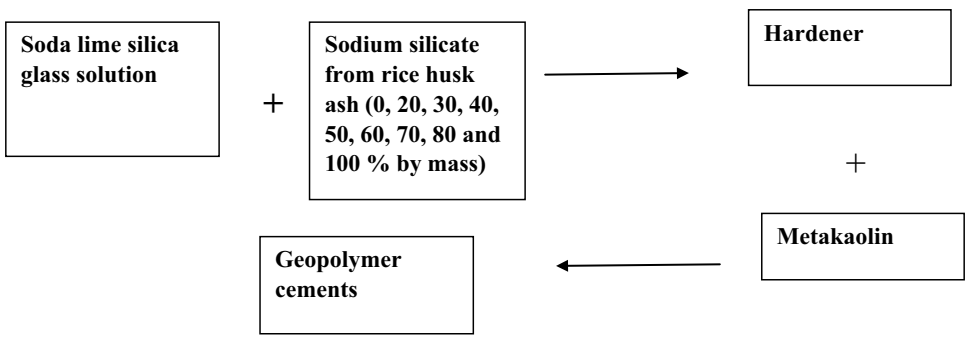

✉ Hervé K. Tchakouté, htchak@yahoo.fr; hervetchakoute@gmail.com | [1]Laboratory of Applied Inorganic Chemistry, Department of Inorganic Chemistry, Faculty of Science, University of Yaounde I, P.O. Box 812, Yaoundé, Cameroon. [2]Faculty of Science, The University of Douala, P.O. Box 24157, Douala, Cameroon. [3]Department of Chemistry in Higher Teacher Training College, University of Maroua, P.O. Box 55, Maroua, Cameroon. [4]Institut für Mineralogie, Leibniz Universität Hannover, Callinstrasse 3, 30167 Hannover, Germany. [5]Laboratory of Analytical Chemistry, Faculty of Sciences, University of Yaounde I, P.O. Box 812, Yaoundé, Cameroon.

SN Applied Sciences (2019) 1:1208 | https://doi.org/10.1007/s42452-019-1242-5

Received: 28 July 2019 / Accepted: 6 September 2019 / Published online: 12 September 2019

Keywords Waste glass · Rice husk ash · Hardeners · Geopolymers · Microstructure · Apparent density

1 Introduction

Geopolymers are new classes of cements for pastes, mortars and concretes that obtained by the addition of an aluminosilicate material with a hardener. The hardeners generally used to depolymerise of this material are sodium or potassium waterglass or phosphoric acid solution. According to the literature, they are new materials for coatings and adhesives, new binders for fibre composites, waste encapsulation, etc. [1]. According to Tittarelli et al. [2], fly ash-based geopolymers are protective for galvanized steel reinforcements. Regarding the environmental impact, the values of hazardous elements classify geopolymers as sustainable materials [3]. But commercial sodium silicate is generally used as a hardener by several researchers for producing geopolymer cements. Whereas, the production of this inorganic polymer has a higher environmental impact which is associated directly with the production of commercial sodium silicate. Hence, the production of this chemical reagent generates a higher amount of greenhouse gas in nature [4–7]. For example, Duxson et al. [8] reported that the total CO_2 emission during the synthesis of commercial sodium silicate is estimated at about 1.514 kg CO_2 emitted per kg of sodium silicate. In order to palliate for this situation and increase the sustainability for the geopolymer production, some researchers used hardeners from raw rice husk ash [9–11], pure rice husk ash [12], sugarcane bagasse ash [13] and waste glass [14–19] for producing geopolymer cements. Regarding sodium waterglass from waste glass, Melele et al. [18] used is to prepare metakaolin-based geopolymer cements cured at room temperature. They reported that the microstructure of the obtained geopolymer cement is heterogeneous, they also exhibit some pores in their structure suggesting the low value of their compressive strength values. They concluded that the lower dissolution of waste glass in the alkaline medium (NaOH) is assigned to the lowest value of its specific surface area (0.91 m^2/g) and the stability of their particle sizes under alkaline solution. This suggests the lower soluble silica content in soda–lime–silica glass solution. In order to improve the dissolution of waste glass, some studies [14–16] reported that the best conditions of solubility of this low-value silica-rich waste were when it used treatment with NaOH and Na_2CO_3. They concluded that Na_2CO_3 favours the dissolution of silica in the waste glass. But, some researchers reported that the manufacture of Na_2CO_3 is energy expensive. For example, Novotny et al. [4] and Fawer et al. [5], reported that the synthesis of sodium carbonate consume a higher amount of energy and generates CO_2 in nature. Hence, the production of commercial sodium waterglass and soda–lime–silica glass solution consume a higher amount of energy and greenhouse gas emitted and therefore reducing significantly their sustainability. In order to avoid the chemical compound Na_2CO_3 during the preparation of soda–lime–silica glass solution and the one of commercial sodium silicate, the combination of the sustainable both hardeners from low-value silica-rich wastes (waste glass and rice husk ash) could reduce the environmental impact.

The main objective of this work is to enhance the reactivity of soda–lime–silica glass solution by adding a different amount of hardener from rice husk ash (0, 20, 30, 40, 50, 60, 70, 80 and 100 wt%) in order to obtain the chemical reagents containing more soluble silica content. The obtained hardeners were used for producing metakaolin-based geopolymer cements. The effect of adding different amount of a chemical reagent from rice husk ash to the one from the waste glass was assessed by the infrared spectroscopy using ATR methods. The reactivity of the obtained hardeners was evaluated by the compressive strengths testing, scanning electron microscope (SEM) observations, X-ray diffractometry (XRD), infrared spectroscopy (IR) using KBr method and the determination of the apparent density of the synthesized geopolymer cements.

2 Materials and experimental methods

2.1 Materials

The kaolin used in this work was collected from Dibamba in the Littoral Region of Cameroon. Waste glass bottles (broken into pieces) and rice husk ash as low-value silica-rich wastes were collected from garbage cans and in Ndop, Department of Ngoketundjia, Region of North-West (Cameroon), respectively. The husks are already calcined in the open air by the company and the white powders of rice husk ash are obtained. Kaolin, rice husk ash and the obtained pieces of waste glass were separately crushed in a ball mill (MGS Sarl) for 1 h. The resulting fine powders of kaolin, rice husk ash and waste glass sieved to 80 µm were labelled Dib_2, RHAB and WGS, respectively. The powder of kaolin was calcined in a programmable electric furnace (MGS Sarl) for 4 h at a heating and cooling rate of 5 °C/min at 700 °C to get metakaolin denoted MK-Dib_2. NaOH pellets with 99% purity were provided by Merck. Rice husk ash, RHAB, was already used by Mabah et al. [20] for the synthesis of the semi-crystalline calcium silicate. They reported that it

mainly constitutes of amorphous silica and α-cristobalite as impurities. The chemical composition of rice husk ash is given in Table 1.

2.2 Experimental methods

2.2.1 Preparation of hardeners

The hardeners from waste glass and rice husk ash were separately prepared by adding NaOH pellets to the powders of each low-value silica-rich wastes. Each blend of waste glass-NaOH and rice husk ash-NaOH was mixed with distilled water and treated for 30 min at 100 °C using a magnetic stirrer. Both hardeners were prepared using the molar ratios SiO_2/Na_2O kept constant at 1.5. The soda–lime–silica glass solution was filtered in order to separate it to the residual waste glass (RWG), i.e. undissolved waste glass. Whereas, rice husk ash is completely dissolved during the preparation of the chemical reagent. The presence of the undissolved particles of WGS implies the significant modification of the values of the molar ratio SiO_2/Na_2O in the reactive ingredient. The soda–lime–silica glass solution and hardener from RHAB are denoted H1 and H9, respectively. In order to improve the reactivity of soda–lime–silica glass solution, the hardener from RHAB, H9, was added to the one of soda–lime–silica glass solution, H1, (0, 20, 30, 40, 50, 60, 70, 80, and 100 wt%). The hardeners from 0, 20, 30, 40, 50, 60, 70, 80, and 100 wt% were labelled H1, H2, H3, H4, H5, H6, H7, H8, and H9, respectively.

Table 1 Chemical compositions of kaolin (Dib_2), rice husk ash (RHAB) and waste glass (WGS), wt%

	Dib_2	RHAB	WGS
Na_2O	< 0.10	–	11.78
MgO	0.10	0.28	1.39
Al_2O_3	25.40	0.58	2.02
SiO_2	59.60	93.20	71.81
P_2O_5	0.078	–	0.024
SO_3	< 0.02	–	0.034
K_2O	0.32	3.05	0.73
CaO	0.18	0.57	11.38
TiO_2	2.21	0.03	0.08
Cr_2O_3	–	–	0.22
Fe_2O_3	2.14	2.20	0.45
ZnO	–	–	0.007
SrO	–	–	0.02
ZrO_2	–	–	0.02
Others	–	1.78	–
LOI	10.25	1.2	0.01
Total	100.40	100.00	99.99

2.2.2 Synthesis of geopolymer cements

Geopolymer cement were prepared by adding each hardener (182.6 g) to metakaolin (220 g) and mixed mechanically for 5 min in order to get the series of specimens GPS0, GPS20, GPS30, GPS40, GPS50, GPS60, GPS70, GPS80, and GPS100 which correspond to the geopolymer cements from the hardeners H1, H2, H3, H4, H5, H6, H7, H8, and H9, respectively. The obtained fresh geopolymer pastes were rapidly moulded into cubic moulds (40 × 40 × 40 mm) and rectangular moulds (40 × 40 x 15 mm) and vibrated mechanically for 2 min. During the hardening process, the specimens were covered with plastic for 24 h at the room temperature (about 30.7 °C) of the laboratory before demolding. Then, the samples were demoulded and maintained for 28 days at 30.7 °C with 58% of humidity prior to measuring the compressive strength.

2.2.3 Methods of characterization of raw materials, hardeners and geopolymer cements

The chemical composition of waste glass and kaolin were determined by X-ray fluorescence machine.

The influence of the adding hardener from rice husk ash to soda–lime–silica glass solution on the microstructure and mechanical properties of geopolymer cements were evaluated. The compressive strengths cured at room temperature for 28 days were measured using an automatic hydraulic press 250 kN (Impact Test Equipment Limited) and loading rate of 0.500 MPa/s using the EN196/01 standards. After compressive strength testing, one part of the fragments of the selected geopolymer cements was crushed and the obtained powders were used to measure X-ray diffractometry (XRD) and Fourier transforms infrared spectroscopy (FT-IR). The other fragments were used for SEM observations.

XRD patterns of the powders of kaolin (Dib_2), metakaolin (MK-Dib_2), waste glass (WGS), residual waste glass (RWG) and the selected geopolymer cements were taken using CuKα radiation between 5° and 80° (2θ) in 7 h in steps of 0.03° (Bruker D4).

Infrared (IR) absorption spectra of the powders (starting materials and geopolymer cements) and hardeners were taken by the KBr (200 mg of KBr, about 1.2 mg of each sample) and ATR methods, respectively using a Bruker Vertex 80_V, 2 cm^{-1}, 32 scans.

Geopolymer samples moulded in the moulds 40 × 40 × 15 mm were used for measuring the apparent density without mercury by Archimedes' method using an automatic instrument (Ceramic Instrument mod. DDA/2) using the DIN-51097 standards.

The selected fragments from the mechanical testing, after gold coating and drying, were used for microstructure

observations using a JEOL JSM-6390A Scanning Electron Microscope (SEM) with an acceleration voltage of 30.0 kV.

3 Results and discussion

3.1 Characterization of raw materials and hardeners, H1–H9

3.1.1 Chemical compositions of kaolin and waste glass

The chemical compositions of kaolin and waste glass are given in Table 1. It appears that Dib_2 and WGS content 59.6 and 71.8 wt% of SiO_2, respectively. Besides SiO_2, Dib_2 content 25.40 wt% of Al_2O_3, whereas WGS content about 11.80 and 11.40 wt% of Na_2O and CaO, respectively (Table 1). The kaolin (Dib_2) used in this work is characterized by a low value of the loss on ignition (i.e. about 10.3 wt%). This indicates the low content of clay minerals. The presence of Fe_2O_3 (2.14 wt%) is responsible for the reddish colour observed for the metakaolin. The amount of TiO_2 (2.21 wt%) could indicate the presence of anatase or rutile. The presence of K_2O is attributed to the minor amount of micaceous or K-feldspars mineral [21].

3.1.2 Mineralogical compositions

Figure 1 indicates the X-ray pattern of rice husk ash (RHAB). This figure shows the diffuse halo diffraction band at between 15° and 45° (2θ) centered at around 28° (2θ) confirming the presence of amorphous silica in the structure of this waste material. Besides this amorphous silica, it also presents the reflection peaks of α-cristobalite.

The X-ray pattern of kaolin (Dib_2) is shown in Fig. 2 and it indicates some reflection peaks of kaolinite, illite, anatase, K-feldspars and quartz. The one of metakaolin (Fig. 2) indicates the same reflection peaks except those of kaolinite which was transformed to metakaolinite during the calcination process. The presence of metakaolinite is confirmed by the broad hump structure that appears at between 15° and 34° (2θ) belongs to the presence of amorphous phases. The X-ray patterns of waste glass (WGS) and residuals waste glass (RWG) are recorded in Fig. 3. Both diffractograms exhibit the diffuse halo structure between 12° and 40° (2θ). In addition to this broad hump structure, the X-ray pattern of the residual waste glass indicates some reflection peaks of thermonatrite ($Na_2CO_3{\cdot}H_2O$) owing to the reaction between the unreacted sodium hydroxide and CO_2 of the atmosphere.

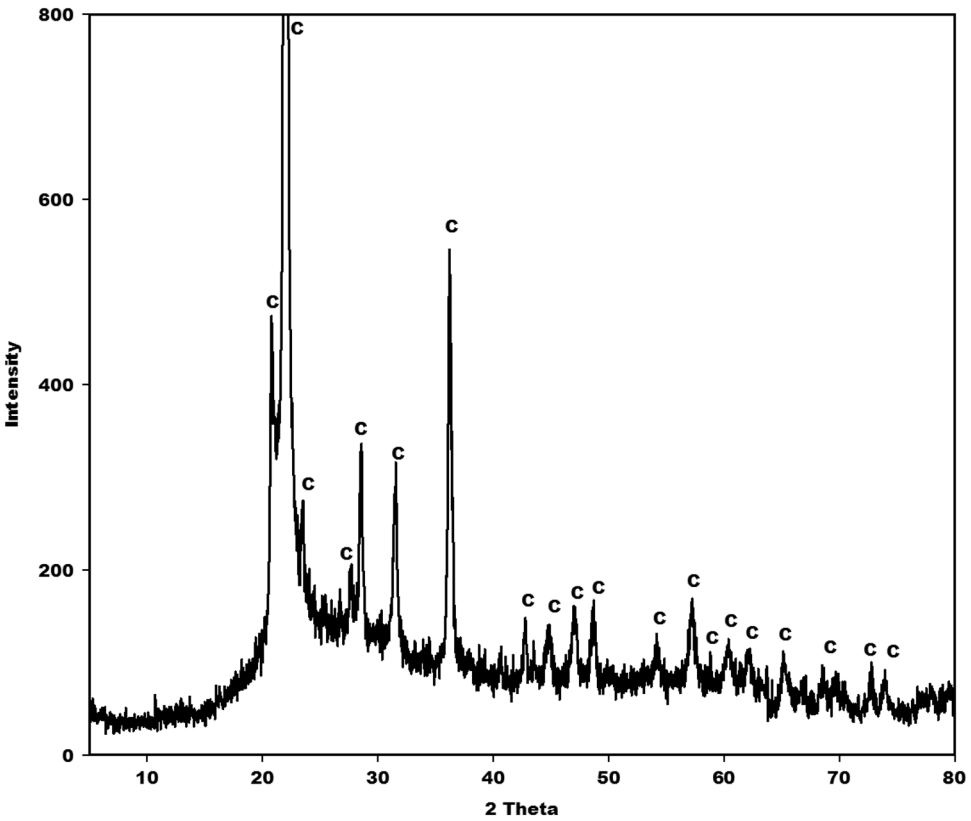

Fig. 1 X-ray pattern of rice husk ash, RHAB. C denote peaks of cristobalite

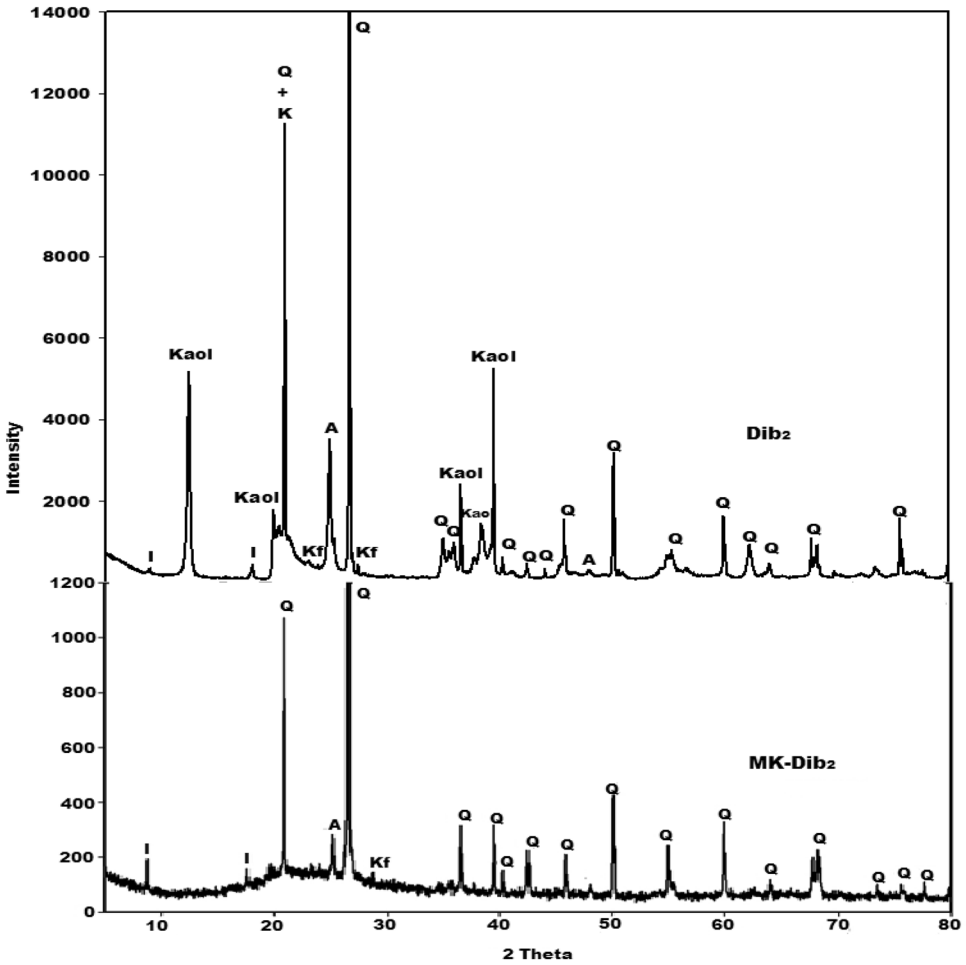

Fig. 2 X-ray patterns of kaolin, Dib_2. Kaol, I, Kf, A and Q denote peaks of kaolinite, illite, K-feldspars, anatase and quartz, respectively

3.1.3 Infrared spectra

The infrared spectrum of rice husk ash is shown in Fig. 4. It appears that the IR spectrum of rice husk ash shows the absorption bands at 470 cm^{-1} which corresponds to the vibration modes of –Si–O–Si– bonds. The one at 792 cm^{-1} is ascribed to the vibration modes of –Si–O–Si– of amorphous and crystalline silica. The band at 1098 cm^{-1} on the IR spectrum of RHAB is associated with the Si–O–Si of amorphous silica. The presence of the amorphous silica at 792 and 1098 cm^{-1} is confirmed on the X-ray pattern RHAB by the presence of the broad hump structure that appears at between 15° and 45° (2θ). The absorption band at 620 cm^{-1} and the shoulder one at 1199 cm^{-1} is attributed to the α-cristobalite. This is consistent with the XRD results. The low intensity of the absorption band at about 1643 cm^{-1} on the IR spectrum of rice husk ash corresponds to the vibration modes of H–O–H of the water molecules.

The infrared spectra of kaolin (Dib_2) and metakaolin ($MK\text{-}Dib_2$) are depicted in Figs. 5 and 6, respectively. The absorption bands at about 3693, 3652 and 3622 cm^{-1} on the IR spectrum of kaolin are the characteristics bands of kaolinite [22–27]. The bands at 467 and 429 cm^{-1} observed on the IR spectra of Dib_2 and $MK\text{-}Dib_2$, respectively are attributed to the bending vibration modes of Si–O–Si bonds [26]. Those at about 542 and 541 cm^{-1} on the IR spectra of the aforementioned starting materials are associated with the bending vibrations of Si–O–Al bonds where Al is in VI-fold coordination [27]. The intensity of this band decreases drastically on the IR spectrum of $MK\text{-}Dib_2$ indicating that during the amorphization of kaolin, Al in VI-fold coordination was transformed to the Al in IV-fold coordination. The one at 911 cm^{-1} on the IR spectrum of Dib_2 belongs to the stretching vibration modes of Al–OH with Al in VI-fold coordination. The absorption band at 754 cm^{-1} on the IR spectrum of Dib_2 is ascribed to the Si–O–Al bonds [26]. The bands at 694 and 795 cm^{-1} on the IR spectrum of Dib_2 and the one at 698 cm^{-1} on the IR spectrum of $MK\text{-}Dib_2$ are ascribed to the bending vibration modes of Si–O–Si bonds of quartz [28]. The one at 795 cm^{-1} on the IR spectrum of kaolin shift to 803 cm^{-1} on the IR spectrum of $MK\text{-}Dib_2$. This could be attributed to the transformation of some crystalline silica to the amorphous silica in the structure of metakaolin. The absorption

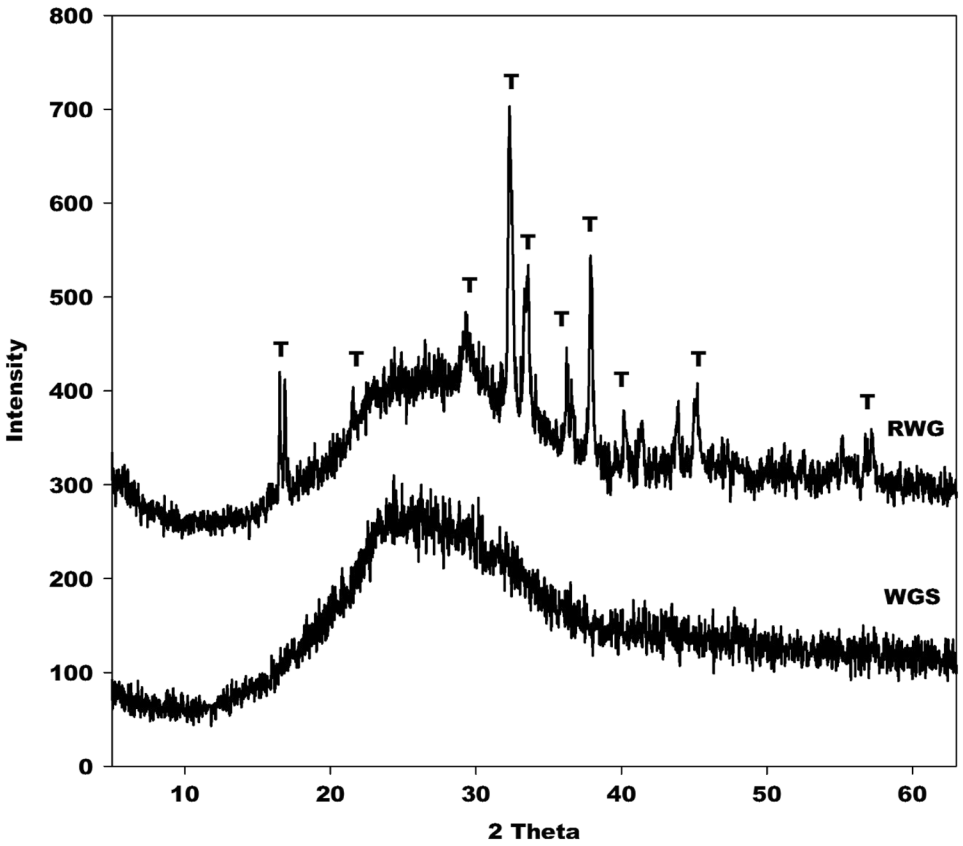

Fig. 3 X-ray patterns of waste glass and remains waste glass, WGS and RWG. T denote peaks of thermonatrite ($Na_2CO_3 \cdot H_2O$)

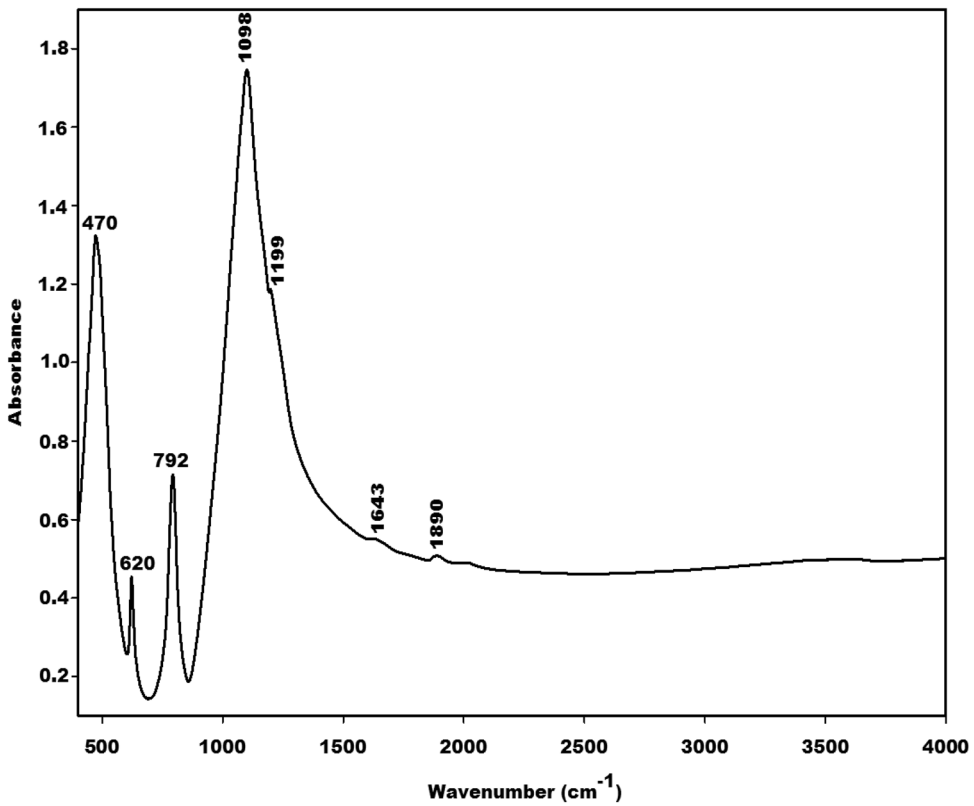

Fig. 4 Infrared spectrum of rice husk ash, RHAB

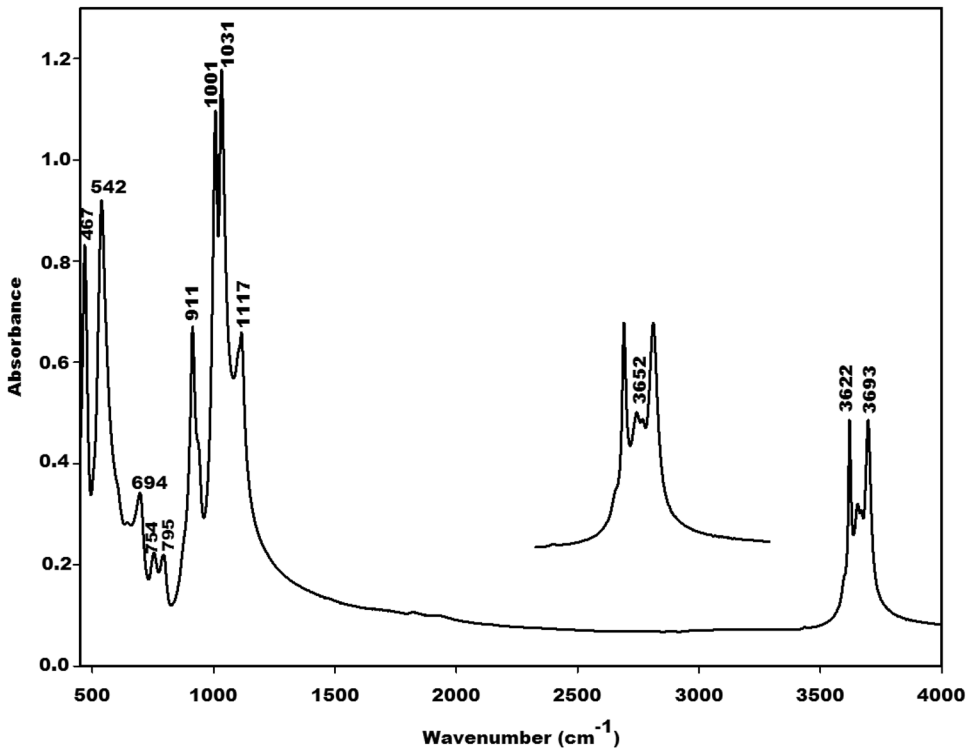

Fig. 5 Infrared spectrum of kaolin (Dib_2)

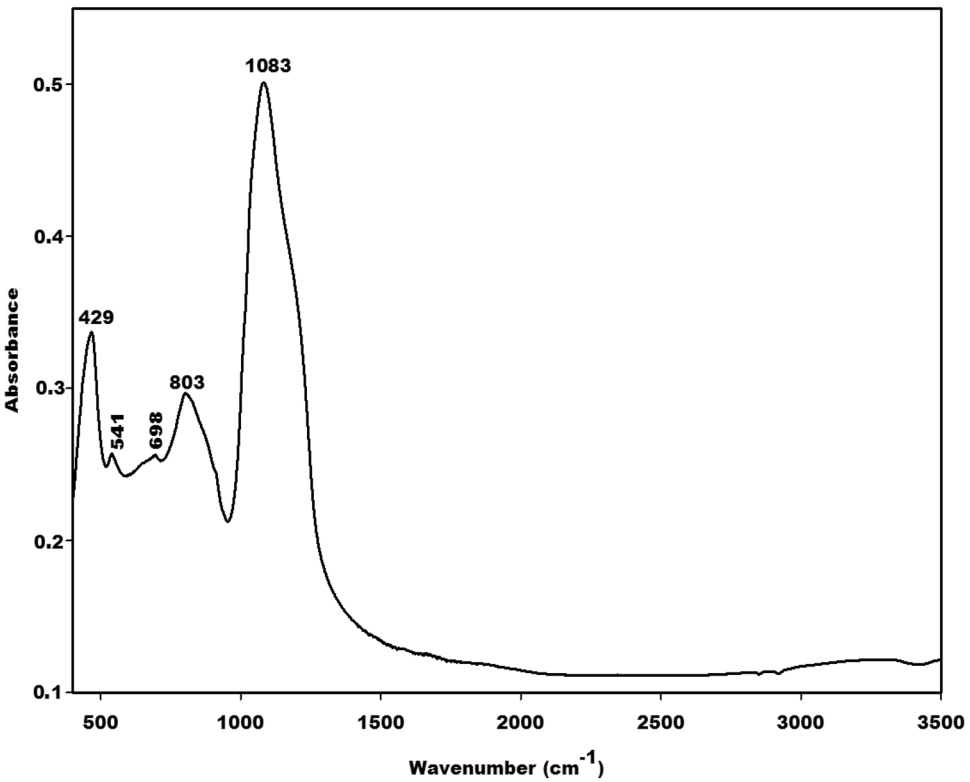

Fig. 6 Infrared spectrum of metakaolin, MK-Dib_2

bands at 1001, 1031 and 1117 cm^{-1} on the IR spectrum of Dib_2 are ascribed to the symmetrical and asymmetrical vibrations of Si–O–Si and Si–O–Al bonds. These bands disappear and the one at 1083 cm^{-1} appears on the IR spectrum of MK-Dib_2 (Fig. 2). The disappearance of the bands at 1001, 1031 and 1117 cm^{-1} and the appearance of the one at 1083 cm^{-1} on the IR spectrum of MK-Dib_2 suggests the transformation of kaolinite to metakaolinite. This

is in agreement with the X-ray pattern of MK-Dib$_2$ which shows the broad hump structure between 15° and 34° (2θ).

The infrared spectra of waste glass (WGS) and residual waste glass (RWG) are exhibited in Fig. 7. The bands at 463 and 452 cm^{-1} on the IR spectra of WGS and RWG, respectively are ascribed to the bending vibration modes of Si–O–Si of glass silica. The band with low intensity at 1445 cm^{-1} observed on the IR spectrum of waste glass are ascribed to the vibration modes of Ca–O. The broad absorption bands at 773 and 1042 cm^{-1} on the IR spectrum of waste glass correspond to the glass phases. The intensity of these bands are lower and the value of the wavenumber of the main band at 1042 cm^{-1} shift to the lower wavenumber 1023 cm^{-1} on the IR spectrum of RWG. The slight shift (i.e. 19 cm^{-1}) towards lower wavenumber indicates the lower dissolution of waste glass particles in the alkaline medium. The lower dissolution of the waste glass justifies the broad hump structure with higher intensity observed on the X-ray pattern of the residual waste glass (Fig. 3). The recent investigation shows that the absorption bands of amorphous silica appear at about 800 and 1100 cm^{-1} [29]. Hence, the lower values of the wavenumber (773 and 1042 cm^{-1}) observed on the IR spectrum of waste glass (Fig. 7) could be related to the incorporation of Ca in the network during the synthesis of the glass. This is confirmed by the absorption band at 1445 cm^{-1} observed on the IR spectrum of waste glass. Those at 1639 and 3454 cm^{-1} on the IR spectrum of WGS are attributed to the H–O–H and O–H of water molecules. The absorption bands at 687, 866, 1411 and 2969 cm^{-1} on the IR spectrum of residual waste glass powder (RWG, (Fig. 7)) is assigned to the CO_3^{2-} ions. Those at 1639 and 3372 cm^{-1} are ascribed to the H–O–H and O–H of water molecules of sodium carbonate monohydrate ($Na_2CO_3{\cdot}H_2O$) observed on the X-ray pattern of RWG (Fig. 3). The presence of the absorption bands of carbonate ions and one of the water molecules confirm the formation of sodium carbonate monohydrate in the structure of RWG. This is also indicated in the X-ray pattern of RWG (Fig. 3) which shows the reflection peaks of $Na_2CO_3{\cdot}H_2O$.

The infrared spectra of soda–lime–silica glass solution (H1), sodium waterglass from rice husk ash (H9) and those obtained by replacement level of H1 (H2, H3, H4, H5, H6, H7 and H8) measured by ATR method are exhibited in Fig. 8. The bands at 3249 and 1647 cm^{-1} observed on the IR spectra of the hardeners H1, H2, H3, H4, H5, H6, H7, H8 and H9 are attributed to the bending vibration modes of O–H and H–O–H, respectively. The main absorption

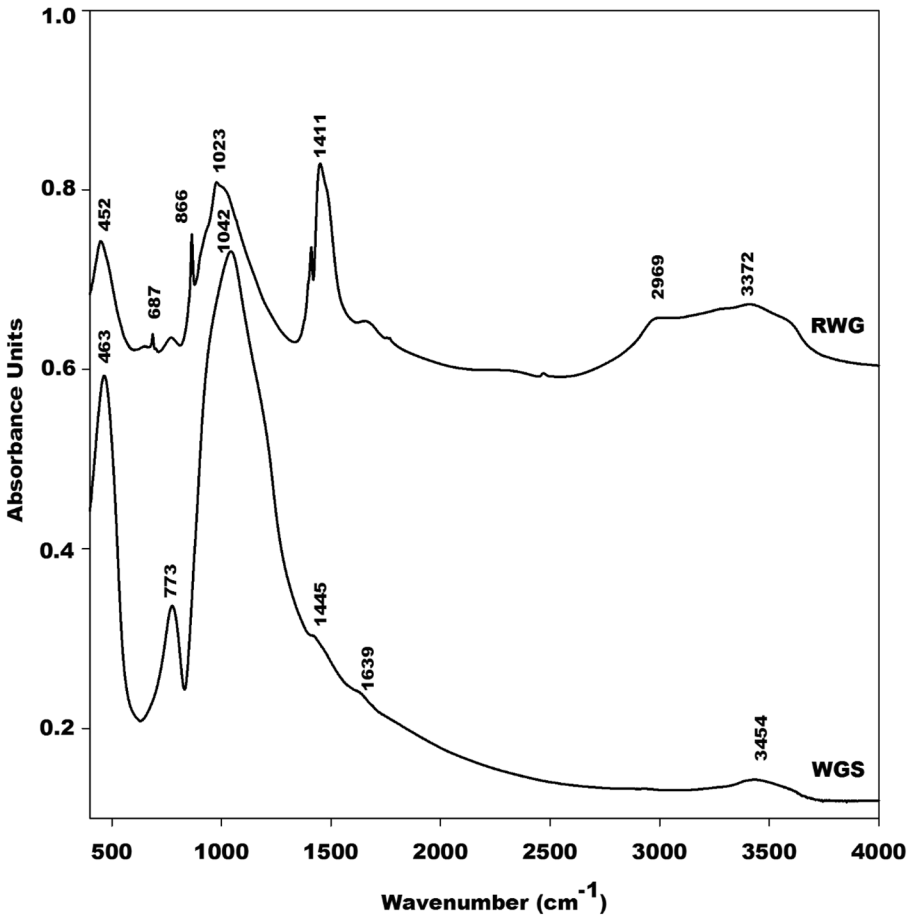

Fig. 7 Infrared spectra of waste glass (WGS) and residual waste glass (RWG)

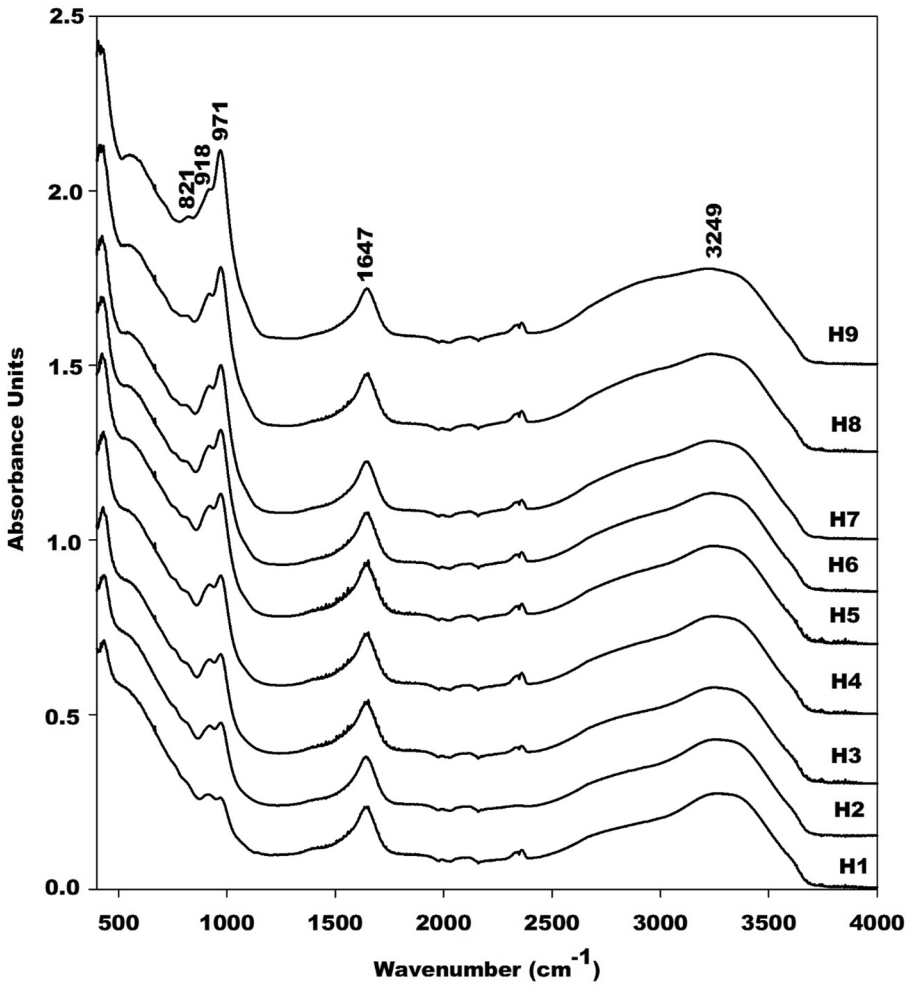

Fig. 8 Infrared spectra of hardeners

bands at about 821, 918, and 971 cm^{-1} observed on the infrared spectra of hardeners are assigned to SiQ^0, SiQ^1 and SiQ^2 units, respectively [11, 12, 17, 30]. The intensity of these bands increases with increasing the amount of H9 added to H1. This indicates that the amount of soluble silicate increases with increasing the addition of the hardener from rice husk ash to the one from waste glass. It is important to notice that this soluble silicate is responsible for the higher degree of depolymerisation of metakaolin. The higher intensity of the absorption band at 971 cm^{-1} implies that SiQ^2 units could play a crucial role during the depolymerisation process of metakaolin.

3.2 Characterization of geopolymer cements

3.2.1 X-ray patterns

The X-ray patterns of the selected geopolymer cements and metakaolin are exhibited in Fig. 9. The X-ray patterns of selected geopolymer cements GPS0, GPS30, GPS50 and GPS100 show the broad hump structure between 18° and 40° (2θ) centered at about 28° (2θ). This broad hump structure appears at a lower value of 2θ on the X-ray pattern of metakaolin (MK-Dib_2). The shift of this diffuse halo structure indicates the formation of the poly(sialate-siloxo) networks. Besides these broad bands, few crystalline reflections peaks of illite, anatase, K-feldspars and quartz are clearly observed on the X-ray patterns of the selected geopolymer cements and metakaolin indicating that these crystalline phases do not react during the polycondensation reaction. The X-ray patterns of geopolymer cements GPS50 and GPS100 show the narrow reflection of the main peak of α-cristobalite at 4.05 Å [20]. This peak is broad on the X-ray pattern of RHAB [20] confirming that the amorphous part contains in the structure of α-cristobalite dissolves during the preparation of hardener H9. This could contribute to enhancing the reactivity of the hardeners leading to the formation of the long chain of poly(sialate-siloxo) network for GPS50, GPS60, GPS70, GPS80 and GPS100. The intensity of the main reflection peak of illite decreases with increasing the amount of H9. This means that,

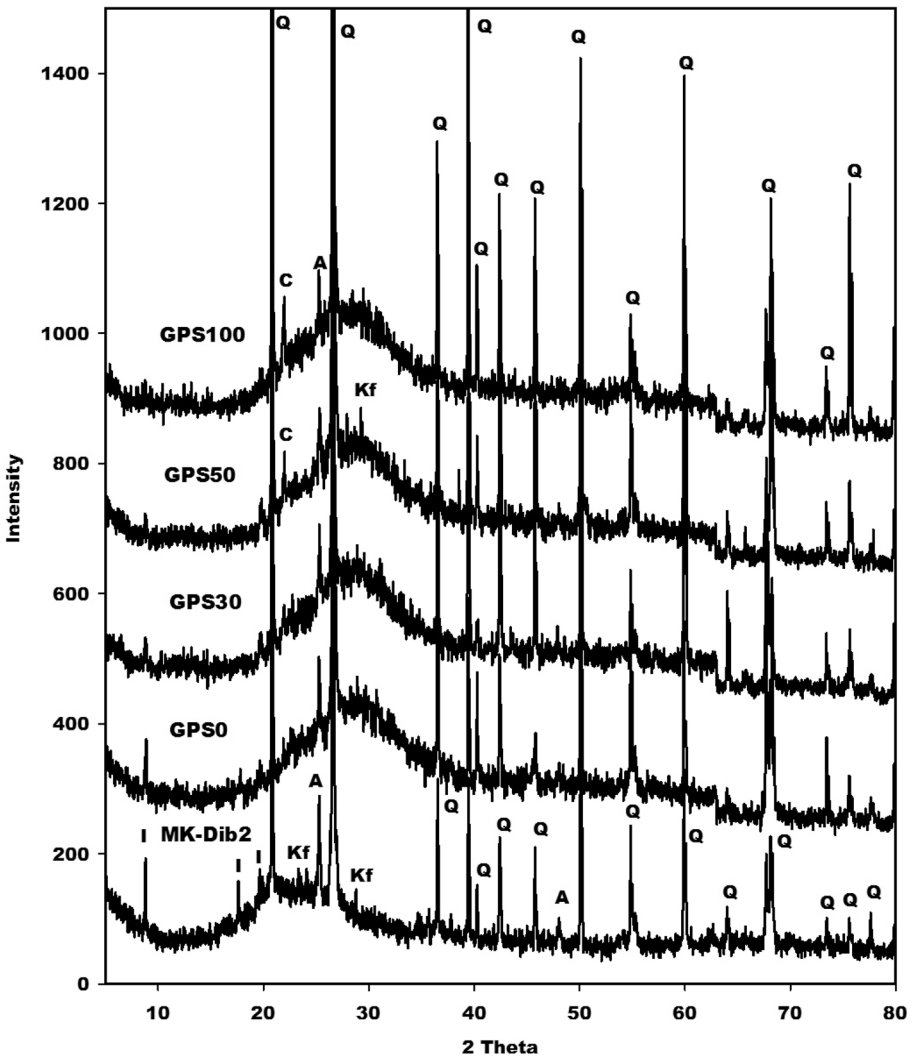

Fig. 9 X-ray patterns of metakaolin (MK-Dib$_2$) and geopolymer cements (GPS0, GPS30, GPS50 and GPS100). I, C, A and Q denote peaks of illite, α-cristobalite, anatase and quartz, respectively

besides metakaolinite, the illite is also dissolved by the high reactivity of the alkaline hardener [30–32].

3.2.2 Infrared spectra

The IR spectra of geopolymer cements GPS0, GPS20, GPS30, GPS40, GPS50, GPS60, GPS70, GPS80, and GPS100 are illustrated in Fig. 10. These spectra show the absorption band at about 448 cm^{-1} which are attributed to the Si–O–Si bonds. This band appears at around 429 cm^{-1} on the IR spectrum of metakaolin (Fig. 6). The shift of this band towards higher wavenumber could be related to the reorganization of the structure of geopolymer cements owing to the depolymerisation of metakaolin and the polycondensation of the precursors formed. The absorption band that appears at 541 cm^{-1} on the IR spectrum of metakaolin disappears on the IR spectra of geopolymer cements. This suggests that during the polycondensation process, Al in VI-fold coordination was transformed into the Al in IV-fold coordination. The one at 687 cm^{-1} is ascribed to the vibration modes of Si–O–Si of quartz. The absorption band at about 721 cm^{-1} corresponds to the vibration modes of Si–O–Al with Al in IV-fold coordination. This band is absent on the IR spectrum of metakaolin indicating the formation of poly(sialate) network in the structure of the final products. The absorption band at about 851 cm^{-1} is assigned to the silanol groups (Si–OH). The one at about 1453 cm^{-1} could be ascribed to C–O of carbonate groups due to the presence of the excess of Na^+ ions which reacts with CO_2 of atmosphere to form Na_2CO_3. The intensity of this band is higher on the IR spectra of GPS0 and GPS20 suggesting the less degree of polycondensation reaction owing to the lower soluble silicate contained in the hardeners H1 and H2. The deficiency of soluble silicate implies the highest concentration of the hardeners H1 and H2 which hinders the polycondensation process. The absorption bands at 3428 and 1666 cm^{-1} are attributed to the deformation and stretching vibration

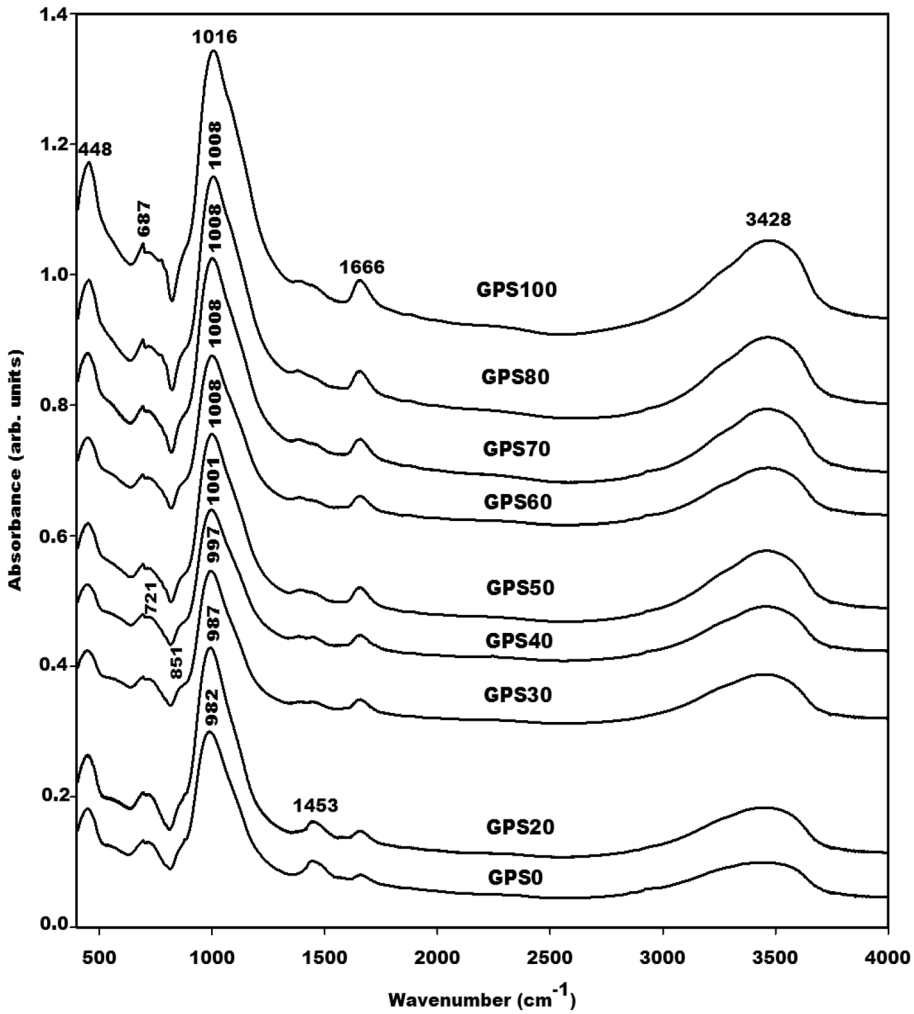

Fig. 10 Infrared spectra of geopolymer cements

modes of O–H and H–O–H, respectively. The main bands of geopolymer cements appears at about 982, 987, 997, 1001, 1008, 1008, 1008, 1008 and 1016 cm^{-1} for GPS0, GPS20, GPS30, GPS40, GPS50, GPS60, GPS70, GPS80, and GPS100, respectively (Fig. 10). These bands are assigned to the asymmetrical and symmetrical stretching vibration modes of siloxo (Si–O–Si) and sialate (Si–O–Al) bonds suggesting thus the formation of the poly(sialate-siloxo) network. The value of the wavenumber of the main absorption band is higher on the infrared spectrum of metakaolin (Fig. 6). The shift of this band towards the lower value of the wavenumber indicates the inclusion of aluminum in the tetrahedral network. This is in agreement with the XRD results which show the displacement of the broad hump structure observed on the X-ray patterns of the selected geopolymer cements (Fig. 9). The inclusion of aluminum in the tetrahedral network is confirmed by the appearance of the absorption band at around 721 cm^{-1}. The lower values of the wavenumbers of the specimens GPS0 (982 cm^{-1}), GPS20 (987 cm^{-1}) and GPS30 (997 cm^{-1}) are related to the higher dissolution of metakaolin due to the higher concentration of the hardeners H1, H2 and H3. This is confirmed by the lower intensities of the bands at 821, 918 and 971 cm^{-1} on the IR spectra of hardeners (Fig. 8) indicating the lower soluble silicate content owing to the lower degree of polycondensation process. This could imply the heterogeneous microstructure, lower values of the apparent density and compressive strengths of GPS0, GPS20 and GPS30. According to Davidovits [1], the hardeners H1, H2 and H3 are not called a user-friendly system, they are hostile system due to their higher concentration (molar ratio SiO_2/Na_2O less than 1.5). However, when hardener from RHAB (H9) is added to the soda–lime–silica glass solution (H1), the values of the wavenumbers of the main absorption bands of geopolymer cements increase. This suggests that the hardeners (H4, H5, H6, H7, H8 and H9) contain a higher amount of soluble silicate leading to a higher degree of polycondensation process. It appears that the higher degree of polycondensation process promotes the higher connectivity of the poly(sialate-siloxo) particles and implies the formation of a highly cross-linking poly(sialate-siloxo) network.

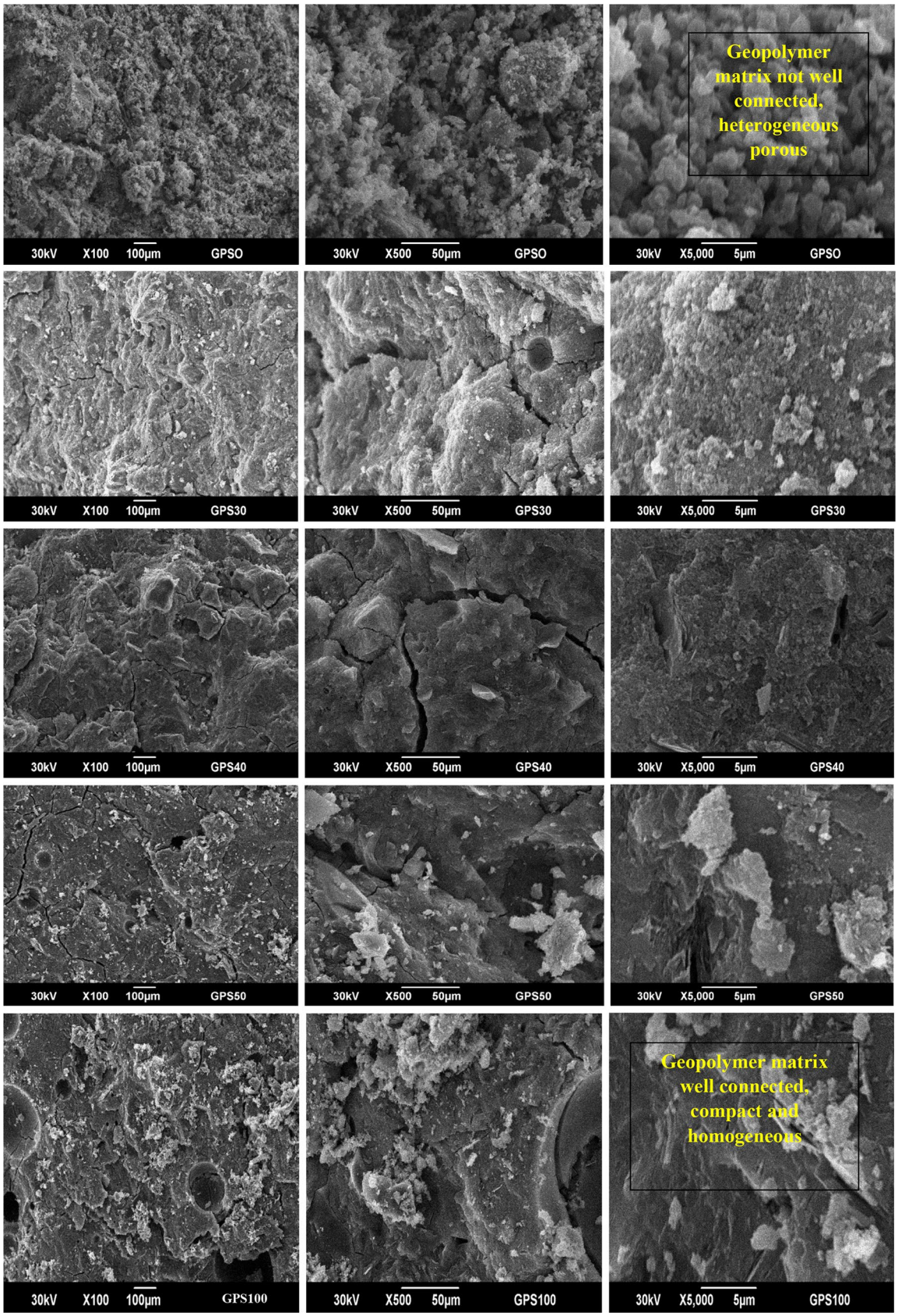

Fig. 11 Micrograph images of the selected geopolymer cements GPS0, GPS30, GPS40, GPS50 and GPS100

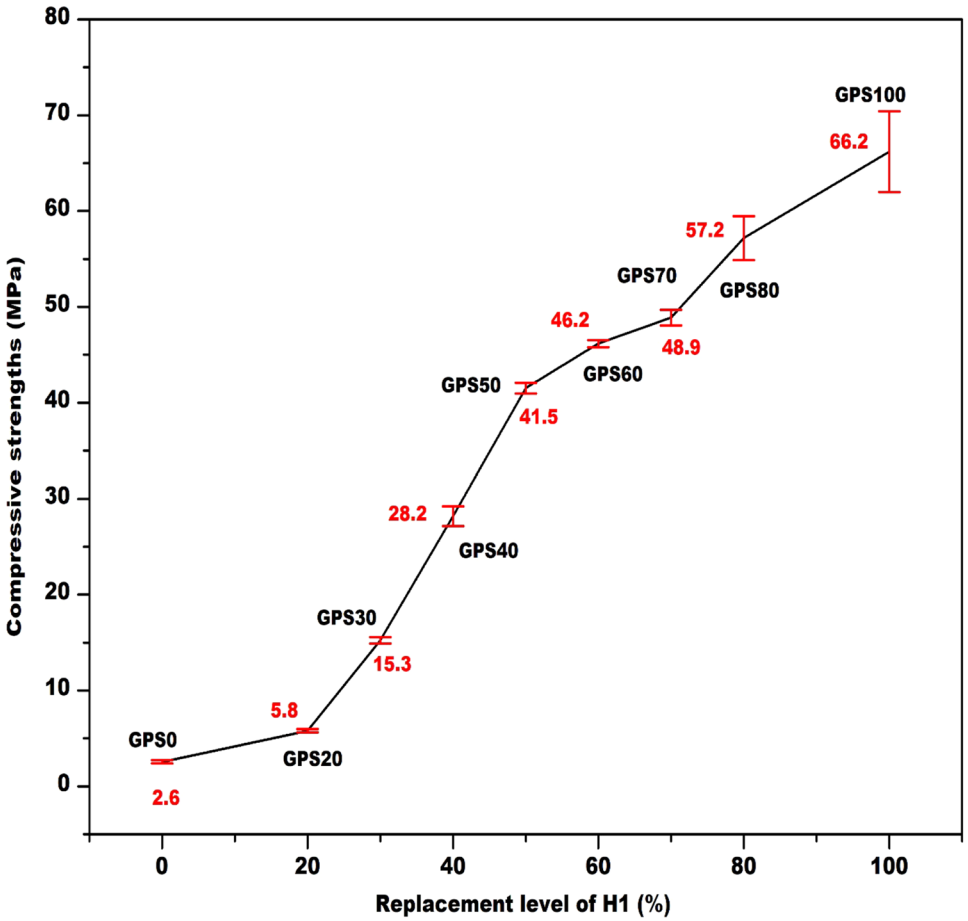

Fig. 12 Compressive strengths of geopolymer cements

3.2.3 Scanning electron microscope (SEM)

The SEM images of the selected geopolymer cements GPS0, GPS30, GPS40, GPS50 and GPS100 are shown in Fig. 11. These images are analysed at 100× 500× and 5000× magnifications. It can be seen that the micrograph images of GPS0 and GPS30 are heterogeneous and exhibit more pores in their structure suggesting the lower values of the apparent density, as discussed below. Whereas the homogeneity of geopolymer cements (GPS40, GPS50 and GPS100) increases with increasing the replacement level of soda–lime–silica glass solution by sodium waterglass from rice husk ash. The microstructure of geopolymer cements goes from porous for geopolymer cements GPS0, GPS20 and GPS30 to the more compact, homogeneous and denser matrix for the specimens GPS40, GPS50, GPS60, GPS70, GPS80 and GPS100. Hence, the increase in the homogeneity of geopolymer cements is clearly observed in the micrograph images analysed at 5000 x magnification. The cracks observed in the micrograph images of GPS30, GPS40, GPS50 and GPS100 could be related to the binder which resists to the load during the compressive strengths testing. This indicates that as soon as 30 wt% of sodium waterglass from rice husk ash (H9) is added to soda–lime–silica glass solution (H1), the poly(sialate-siloxo) network starts to connect and therefore withstand at the load leading to the formation of cracks during the compressive strength measurements. The absence of this crack in the micrograph of GPS0 implies the lowest amount of binder or lowest chain of poly(sialate-siloxo) network.

3.2.4 Compressive strengths

The values of the compressive strengths of geopolymer cements as function as the replacement level of soda–lime–silica glass solution are recorded in Fig. 12. It can be seen that the compressive strengths increase with increasing the replacement level of soda–lime–silica glass solution. According to Fig. 12, the compressive strengths of the specimens denoted GPS0, GPS20, GPS30, GPS40, GPS50, GPS60, GPS70, GPS80 and GPS100 are 2.6, 5.8, 15.3, 28.2, 41.5, 46.2, 48.9, 57.2 and 66.2 MPa, respectively. The lowest values of the compressive strengths of GPS0 and GPS20 could be recorded to the lowest molar ratio SiO_2/Na_2O contained in the chemical ingredient H1, H2 and H3

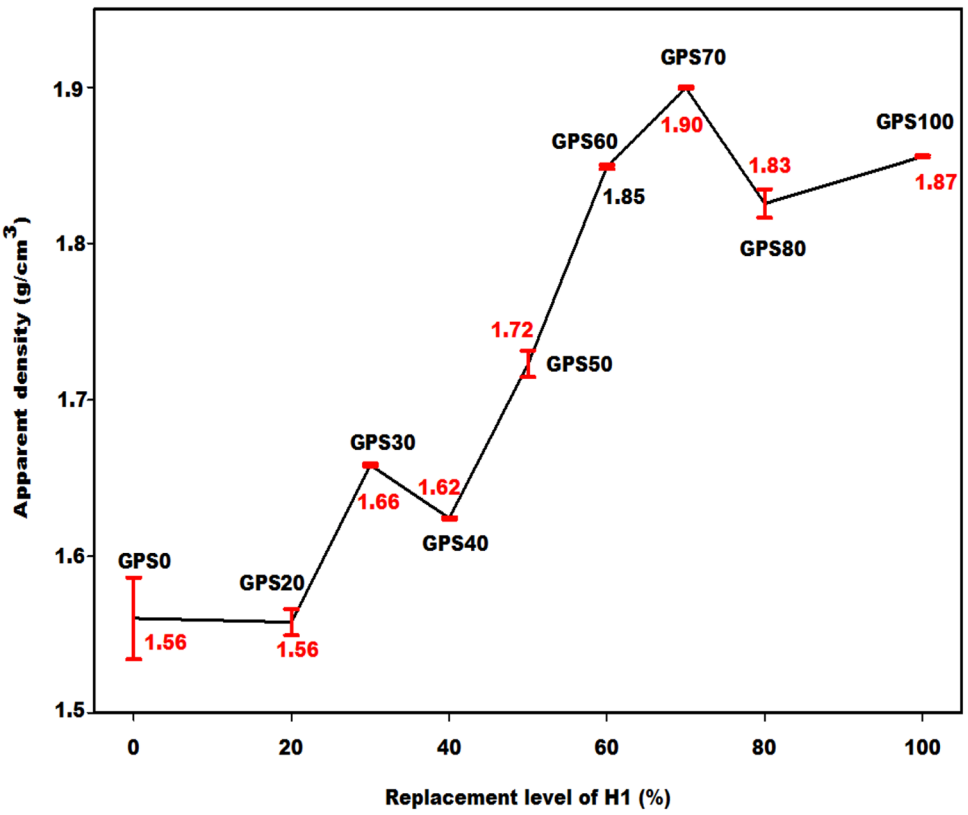

Fig. 13 Apparent density of geopolymer cements

which is associated with the lowest amount of soluble silicate in the aforementioned hardeners. The lowest amount of soluble silicate leads to the formation of the heterogeneous, porous and lowest chain of poly(sialate-siloxo) network, as can be confirmed by the micrograph images of GPS0, GPS20 and GPS30 (Fig. 11). Although the IR spectra of GPS0, GPS20 and GPS30 show also the formation of the absorption band at about 728 cm^{-1}, the compressive strengths of these specimens are very low confirming the formation of the heterogeneous and lowest chain of poly(sialate-siloxo) network. This lowest chain is related to the presence of the absorption band at 1453 cm^{-1} with a slightly higher intensity which hinders the polycondensation process owing to the deficiency of the soluble silicate in the hardeners H1, H2 and H3.

3.2.5 Apparent density

Figure 13 exhibits the apparent density of geopolymer cements as function as the replacement level of soda–lime–silica glass solution (H1). It seems that the values of the apparent density increase with increasing the replacement level of soda–lime–silica glass solution. This implies the progressive formation of the denser matrix (Fig. 11) corresponding to the increase of the values of the compressive strengths (Fig. 12) and also the formation of a long chain of poly(sialate-siloxo) network. The low values of the apparent density of GPS40 compared to GPS30, and the one of GPS80 compared to GPS70 could be ascribed to the mechanically vibrating which induces the formation of a capillary air bubble in the network, as can be shown in Fig. 11. The lowest values of apparent density of GPS0 and GPS20 (1.56 g/cm^3) compared to the others could be related to the formation of more pores (as clearly shown in Fig. 11 for GPS0) and the low chain of poly(sialate-siloxo) network. This is in agreement with the lower values of the wavenumber of the main bands of GPS0 (982 cm^{-1}) and GPS20 (987 cm^{-1}) observed on the IR spectra of geopolymer cements (Fig. 10) and confirms that the addition of the chemical ingredient from rice husk ash (H9) to soda–lime–silica glass solution (H1) brings the additional soluble silicate in the hardeners. The additional soluble silicate contributes to the formation of a long chain of poly(sialate-siloxo) network and justified by the increase of the values of the wavenumber of the main bands of geopolymer cements from 982 to 1016 cm^{-1} (Fig. 10).

4 Conclusion

The sustainable hardeners were prepared using the low-value silica-rich wastes like rice husk ash and waste glass. The hardener from rice husk ash has been used as

an additive (0, 20, 30, 40, 50, 60, 70, 80 and 100 wt%) for improving the reactivity of the soda–lime–silica glass solution. The infrared spectrum of soda–lime–silica glass solution shows the lowest intensity of the absorption bands at about 821, 918 and 971 cm^{-1} indicating the lowest amount of soluble silica. This is confirmed by the higher intensity of the broad hump structure observed between 18° and 40° (2θ) on the X-ray pattern and the higher value of the wavenumber of the main band which appears at 1023 cm^{-1} on the infrared spectrum of the residual waste glass. The addition of 0, 20, 30, 40, 50, 60, 70, 80 and 100 wt% of the hardener from rice husk ash increases the soluble silica content in the soda–lime–silica glass solution and therefore increases its reactivity. The compressive strengths of geopolymer cements using hardeners from replacement level of soda–lime–silica glass solution 0 (GPS0), 20 (GPS20), 30 (GPS30), 40 (GPS40), 50 (GPS50), 60 (GPS60), 70 (GPS70), 80 (GPS80) and 100% (GPS100) are 2.6, 5.8, 15.3, 28.2, 41.5, 46.2, 48.9, 57.2 and 66.2 MPa, respectively. They increase with increasing the replacement level of soda–lime–silica glass solution. The values of the apparent densities of geopolymer cements increase with increasing the replacement level of soda–lime–silica glass solution. The increase in the values of the density of state peak maximum of geopolymer cements from 982 to 1016 cm^{-1} could be related to the progressive formation of a long chain of poly(sialate-siloxo) network. The micrograph images of geopolymer cements GPS40, GPS50, and GPS100 are homogeneous, compact and denser microstructure. It was typically found that the addition of about 50 or 60 wt% of the chemical ingredient from rice husk ash could be used for producing sodium waterglass which can be used to synthesize geopolymer cements with the compressive strength equal to 41.2 or 46.2 MPa that can be compared to the one from Portland cement CEM I (42.5 MPa). We can conclude that the reactivity of soda–lime–silica glass solution can be improved by adding hardener from rice husk ash and used it for producing geopolymer cements with higher compressive strengths, denser matrix, homogeneous and compact microstructure. The addition of the hardener from rice husk ash to the soda–lime–silica glass solution is viewed as a viable and cleaner solution to optimize the reactivity of chemical ingredient from waste glass and therefore improve the sustainability of geopolymer cements, mortars and concretes. The low values of the apparent density (1.56 g/cm^3) and the compressive strength (2.6 MPa) of geopolymer cement from soda–lime–silica glass solution, GPS0, could indicate that soda-lime glass solution (H1) could be used for producing sustainable lightweight geopolymer cements.

Acknowledgements Hervé K. Tchakouté gratefully acknowledges the Alexander von Humboldt Foundation for financial support this work under the Grant No. KAM/1155741 GFHERMES-P. The authors would like to thank Mr. Valerie Petrov for SEM observation.

Compliance with ethical standards

Conflict of interest On behalf of all authors, the corresponding author states that there is no conflict of interest.

References

1. Davidovits J (2011) Geopolymer chemistry and applications, 3rd edn. Institute Geopolymer, Saint-Quentin, p 612
2. Tittarelli F, Mobili A, Giosuè C, Belli A, Bellezze T (2018) Corrosion behaviour of bare and galvanized steel in geopolymer and Ordinary Portland Cement based mortars with the same strength class exposed to chlorides. Corros Sci 134:64–77
3. Coppola L, Bellezze T, Belli A, Bignozzi MC, Bolzoni F, Brenna A et al (2018) Binders alternative to Portland cement and waste management for sustainable construction—part 1. J Appl Biomater Funct Mater 16:186–202
4. Novotny R, Hoff A, Schuertz J (1991) Process for hydrothermal production of sodium silicate solutions. United States Patent, No 5000933
5. Fawer M, Concannon M, Rieber W (1999) Life cycle inventories for the production of sodium silicates. Int J Life Cycle Assess 4:207–212
6. Witherspoon R, Wang H, Aravinthan T, Omar T, (2009) Energy and emissions analysis of fly ash based geopolymers. In: SSEE international conference-solutions for a sustainable planet, society for sustainability and environment engineering, Melbourne, VIC, p 29
7. Tempest B, Sanusi O, Gergely J, Ogunro V, Weggel D (2009) Compressive strength and embodied energy optimization of fly ash based geopolymer concrete. In: Proceedings of the world of coal ash (WOCA) conference, Lexington, KY
8. Duxson P, Mallicoat SW, Lukey GC, Kriven WM, van Deventer JSJ (2007) The effect of alkali and Si/Al ratio on the development of mechanical properties of metakaolin-based geopolymers. Colloids Surf A Physicochem Eng Asp 292:8–20
9. Bernal SA, de Gutierrez EDRM, Provis JL, Delvasto S (2012) Activation of metakaolin/slag blends using alkaline solutions based on chemically modified silica fume and rice husk ash. Waste Biomass Valoriz 3:99–108
10. Kamseu E, Beleuk à Moungam LM, Cannio M, Billong N, Chaysuwan D, Melo FUC, Leonelli C (2016) Substitution of sodium silicate with rice husk ash-NaOH solution in metakaolin-based geopolymer cement concerning reduction in global warming. J Clean Prod 142:3050–3060
11. Tchakouté HK, Rüscher CH, Kong S, Kamseu E, Leonelli C (2016) Comparison of metakaolin-based geopolymer cements from commercial sodium waterglass and sodium waterglass from rice husk ash. J Sol–Gel Sci Technol 78:492–506
12. Tchakouté HK, Rüscher CH, Kong S, Ranjbar N (2016) Synthesis of sodium waterglass from white rice husk ash as an activator to produce metakaolin-based geopolymer cements. J Build Eng 6:252–261
13. Tchakouté HK, Rüscher CH, Hinsch M, Djobo JNY, Kamseu E, Leonelli C (2017) Utilization of sodium waterglass from sugar cane bagasse ash as a new alternative hardener for producing

metakaolin-based geopolymer cement. Chem der Erde Geochemist 77:257–266
14. Puertas F, Torres-Carrasco M (2014) Use of glass waste as an activator in the preparation of alkali-activated slag. Mechanical strength and paste characterization. Cem Concr Res 57:95–104
15. Torres-Carrasco M, Palomo JG, Puertas F (2014) Sodium silicate solutions from dissolution of glass wastes. Statistical analysis. Mater Constr 64:1–14
16. Torres-Carrasco M, Puertas F (2015) Waste glass in the geopolymer preparation. Mechanical and microstructural characterisation. J Cleaner Prod 90:397–408
17. Tchakouté HK, Rüscher CH, Kong S, Kamseu E, Leonelli C (2016) Geopolymer binders from metakaolin using sodium waterglass from waste glass and rice husk ash as alternative activators: a comparative study. Constr Build Mater 114:276–289
18. Melele SJK, Tchakouté HK, Banenzoué C, Kamseu E, Rüscher CH, Andreola F, Leonelli C (2018) Investigation of the relationship between the condensed structure and the chemically bonded water content in the poly(sialate-siloxo) network. Appl Clay Sci 156:77–86
19. Toniolo N, Rincón A, Roether JA, Ercole P, Bernardo E, Boccaccini AR (2018) Extensive reuse of soda-lime waste glass in fly ash-based geopolymers. Constr Build Mater 188:1077–1084
20. Mabah DET, Tchakouté HK, Rüscher CH, Kamseu E, Elimbi A, Leonelli C (2019) Design of low cost semi-crystalline calcium silicate from biomass for the improvement of the mechanical and microstructural properties of metakaolin-based geopolymer cements. Mater Chem Phys 223:98–108
21. Monteiro SN, Vieira CMF, Peçanha LA (2004) Reformulation of roofing tiles body with addition of granite waste from sawing operations. J Eur Ceram Soc 24:2349–2356
22. Van der Marel HW, Beutelspacher H (1977) Atlas of infrared spectroscopy of clay minerals and their admixtures. Clay Miner 12:279–280
23. Russel JD (1987) Infrared spectroscopy of inorganic compounds, Laboratory methods infrared spectroscopy. Wiley, New York
24. Kakali G, Tsivilis T, Badogiannis E (2001) Thermal treatment of kaolin: the effect of mineralogy on the pozzolanic activity. Appl Clay Sci 20:73–80
25. Mohammad QA, Naji Al-Trawneh I (2005) Characterization of kaolinite of the Bten El-Ghoul region south Jordan by infrared spectroscopy. Spectrochem Acta Part A 61:1519–1523
26. Tironi A, Trezza MA, Scian AN, Irassar EF (2012) Kaolinitic calcined clays: factors affecting its performance as pozzolans. Constr Build Mater 28:276–281
27. Tironi A, Trezza MA, Irassar EF, Scian AN (2012) Thermal treatment of kaolin: effect on the pozzolanic activity. Procedia Mater Sci 1:343–350
28. Tchakouté HK, Rüscher CH, Djobo JNY, Kenne BBD, Njopwouo D (2015) Influence of gibbsite and quartz in kaolin on the properties of metakaolin-based geopolymer cements. Appl Clay Sci 107:188–194
29. Rees CA, Provis JL, Lukey GC, van Deventer JSJ (2007) In situ ATR-FTIR study of the early stages of fly ash geopolymer gel formation. Langmuir 23:9076–9082
30. Gharzouni A, Joussein E, Samet B, Baklouti S, Pronier S, Sobrados I, Sanz J, Rossignol S (2015) The effect of an activation solution with siliceous species on the chemical reactivity and mechanical properties of geopolymers. J Sol–Gel Sci Technol 73:250–259
31. Buchwald A, Hohmann M, Posern K, Brendler E (2009) The suitability of thermally activated illite/smectite clay as raw material for geopolymer binders. Appl Clay Sci 46:300–304
32. Zibouche F, Kerdjoudj H, d'Espinose de Lacaillerie J-B, Van Damme H (2009) Geopolymers from Algerian metakaolin. Influence of secondary minerals. Appl Clay Sci 43:453–458